UCSF
UC San Francisco Previously Published Works

Title
Anion transport inhibitor binding to band 3 in red blood cell membranes.

Permalink
https://escholarship.org/uc/item/3zh727z4

Journal
The Journal of General Physiology, 81(3)

ISSN
0022-1295

Authors
Verkman, AS
Dix, JA
Solomon, AK

Publication Date
1983-03-01

DOI
10.1085/jgp.81.3.421

Peer reviewed

eScholarship.org Powered by the California Digital Library
University of California

Anion Transport Inhibitor Binding to Band 3 in Red Blood Cell Membranes

A. S. VERKMAN, JAMES A. DIX, and A. K. SOLOMON

From the Biophysical Laboratory, Department of Physiology and Biophysics, Harvard Medical School, Boston, Massachusetts 02115

ABSTRACT The inhibitor of anion exchange 4,4′-dibenzoamido-2,2′-disulfonic stilbene (DBDS) binds to band 3, the anion transport protein in human red cell ghost membranes, and undergoes a large increase in fluorescence intensity when bound to band 3. Equilibrium binding studies performed in the absence of transportable anions show that DBDS binds to both a class of high-affinity (65 nM) and low-affinity (820 nM) sites with stoichiometry equivalent to 1.6 nmol/mg ghost protein for each site, which is consistent with one DBDS site on each band 3 monomer. The kinetics of DBDS binding were studied both by stopped-flow and temperature-jump experiments. The stopped-flow data indicate that DBDS binding to the apparent high-affinity site involves association with a low-affinity site (3 μM) followed by a slow (4 s^{-1}) conformational change that locks the DBDS molecule in place. A detailed, quantitative fit of the temperature-jump data to several binding mechanisms supports a sequential-binding model, in which a first DBDS molecule binds to one monomer and induces a conformational change. A second DBDS molecule then binds to the second monomer. If the two monomers are assumed to be initially identical, thermodynamic characterization of the binding sites shows that the conformational change induces an interaction between the two monomers that modifies the characteristics of the second DBDS binding site.

INTRODUCTION

The anion exchange system of the human red cell is mediated by a glycoprotein, band 3, of ~95,000 daltons. Band 3 makes up ~25% of the total red cell membrane protein and is present in the membrane as ~550,000 noncovalent dimers. Anion exchange is thought to occur via a conformational change that translocates anion binding sites between external and cytoplasmic membrane interfaces. A number of disulfonic stilbenes have been used to probe the structure and function of band 3 (for reviews, see Steck, 1978; Cabantchik et al., 1978; Knauf, 1979). One of these compounds, 4,4′-diisothiocyano-2,2′-disulfonic stilbene (DIDS), completely inhibits anion exchange by reacting at one site per band 3 monomer (Ship et al., 1977; Lepke et al., 1976). A

Address reprint requests to Dr. A. S. Verkman, Harvard Medical School, Biophysical Laboratory, 25 Shattuck St., Boston, MA 02115.

J. GEN. PHYSIOL. © The Rockefeller University Press · 0022-1295/83/03/0421/29 $1.00 421

Volume 81 March 1983 421–449

fluorescent DIDS analogue, 4,4′-dibenzoamido-2,2′-disulfonic stilbene (DBDS), binds reversibly and specifically to the DIDS-reactive site, where it also inhibits anion exchange (Cabantchik and Rothstein, 1972; Rao et al., 1979). As first shown by Cabantchik and Rothstein (1972), the fluorescence intensity of DBDS increases by two orders of magnitude when bound to band 3 in red cell membranes. Resonance energy transfer measurements (Rao et al., 1979) show this site to be 34–42 Å from the cytoplasmic domain of band 3.

We have studied the binding of DBDS to red cell ghost membranes by equilibrium binding and temperature-jump techniques (Dix et al., 1979). In the absence of transportable anions, we found that DBDS binds to both a high-affinity site and a low-affinity site on ghost membranes with approximately equal stoichiometry and we put forward the following minimal mechanism for the binding in the absence of transportable anions:

$$\begin{array}{ccccccc} \text{band 3} & \overset{K_1}{\rightleftharpoons} & \text{band 3-DBDS} & \underset{k_{-2}}{\overset{k_2}{\rightleftharpoons}} & \text{band 3*-DBDS} & \overset{K_3}{\rightleftharpoons} & \text{band 3*-(DBDS)}_2 \\ & \searrow\!\!\downarrow & & & & \searrow\!\!\downarrow & \\ & \text{DBDS} & & & & \text{DBDS} & \end{array} \qquad (1)$$

in which band 3 represents a band 3 dimer and the bimolecular steps are considered to be fast compared with the conformational change.

We have now made more detailed studies of the equilibrium binding of DBDS using both fluorescence enhancement and centrifugation techniques and have found that the association constant for binding to both sites depends logarithmically on (ionic strength)$^{1/2}$. We have also used the stopped-flow method to supplement the information about the kinetics previously obtained by the temperature-jump technique. On the basis of all this information, we have made a critical examination of a number of alternative models for the DBDS binding mechanism and found that the model given in Eq. 1 is a satisfactory, simple model, with the additional assumption that the first bimolecular association is slower than initially assumed. We then used the kinetic and equilibrium data that describe this model to generate the appropriate thermodynamic parameters for the system.

MATERIALS AND METHODS

Reagents

DBDS was synthesized by the method of Kotaki et al. (1971) and its purity was checked by thin-layer chromatography on Silica Gel G (Whatman, Inc., Clifton, NJ) in pyridine:acetic acid:water (10:1:40). DIDS was purchased from Pierce Chemical Co. (Rockford, IL) and was used without further purification. DNDS (4,4′-dinitro-2,2′-disulfonic stilbene) was purchased from K & K Laboratories of ICN Pharmaceuticals (Plainview, NY). DBDS was stored as 1-mM aqueous solutions at 4°C in the dark. DIDS and DNDS solutions were prepared immediately before use and DNDS was kept in the dark. All other chemicals were purchased from Sigma Chemical Co. (St. Louis, MO).

Membrane Preparations

Hemoglobin-free unsealed red cell ghosts were prepared by a method similar to that of Dodge et al. (1963). Recently outdated blood was washed three times in 155 mM NaCl, hemolyzed in 5 mM sodium phosphate at pH 8.0, washed four times in the phosphate buffer, and then washed twice in the buffer used for subsequent experiments. Ghosts were generally used within 24 h of preparation, although longer storage did not affect the results of kinetic experiments. Red cell lipids were extracted from ghosts by the method of Roelofsen et al. (1974) and stored at −20°C in ethanol. Right-side-out vesicles were prepared by the method of Steck and Kant (1974).

Unilamellar vesicles were prepared by sonication using the method of Huang and Thompson (1974). Red cell lipids were rotary evaporated to remove ethanol and suspended in buffer at a lipid concentration of ~25 mM. The suspension was sonicated at 4°C under N_2 for 1 h using a Branson model W 185 sonicator (Heat Systems-Ultrasonics, Inc., Plainview, NY). The vesicles were then centrifuged at 40,000 *g* for 45 min to remove titanium particles in a Sorvall model RC2-B refrigerated centrifuge (DuPont Instruments-Sorvall, Newtown, CT). Vesicles were stored under N_2 at 5°C and used within 1 wk of preparation.

Equilibrium Binding Studies

The equilibrium binding of DBDS to red cell ghosts was measured as described previously (Dix et al., 1979). Ghosts were incubated with known concentrations of DBDS for 1 h in 28.5 mM sodium citrate, pH 7.4, 25°C, and then centrifuged at 40,000 *g* for 30 min. The concentration of DBDS in the supernatant was determined by absorption at 336 nm or by fluorescence enhancement (excitation 350 nm, emission 435 nm) on addition of either 0.08% bovine serum albumin or 0.04 mg/ml red cell ghosts. The quantity of bound DBDS was determined from the difference between total DBDS added and free DBDS. The ghost concentration varied between 0.4 and 1.3 mg/ml protein as determined by the Lowry assay (Lowry et al., 1951).

A second method used to measure the binding of DBDS to ghost membranes was fluorescence enhancement titration in which the fluorescence of bound DBDS was used as a sensitive indicator of binding. Known concentrations of DBDS were added to a dilute ghost solution (0.02 mg/ml); fluorescence was excited at 350 nm and monitored at 427 nm in a fluorescence spectrophotometer interfaced to a PDP 11/34 computer (Digital Equipment Corp., Maynard, MA) (Kleinfeld et al., 1979). The fluorescence data were analyzed as described in the Appendix. The fluorescence enhancement titration method is significantly faster than the centrifugation method. Consequently, it is possible to obtain many more points by fluorescence enhancement titration so that this method has become our method of choice in the binding affinity studies.

Substituted stilbenes are known to undergo *cis-trans* photoisomerization (DeTar and Carpino, 1956; Schulte-Frohlinde et al., 1962). The *cis* form of DIDS is reported to be half as potent an anion transport inhibitor as the *trans* form (Ship et al., 1977); the *cis* form of DNDS has a binding affinity many orders of magnitude less than the *trans* form (Fröhlich and Gunn, 1980). In view of these findings, we studied the *cis-trans* isomerization of DBDS. 10 μM of DBDS, DIDS, and DNDS in 28.5 mM citrate buffer was irradiated for 5 min by placing a cuvette 20 cm from a 150-W Hg arc lamp in the absence of the monochromator; isomerization was determined by the decrease in absorbance at the wavelength corresponding to the *trans* form (DBDS: 336 nm; DIDS: 344 nm; DNDS: 350 nm). The absorbance decreased 20% for DIDS and 45% for DNDS, but only 2% for DBDS. Prolonged irradiation (>2 h) of the DBDS

sample produced an absorbance at 280 nm, corresponding to the *cis* form of DBDS. The Hg lamp used in the *cis-trans* experiments was the same as that used in the kinetic experiments in which the light intensity was very much attenuated by the monochromator. Since the maximum exposure to light was <1 min in any of our experiments, the data reported in this paper pertain only to the *trans* form of DBDS.

Temperature-Jump Studies

Temperature-jump studies as described by Eigen and DeMaeyer (1974) were performed on an apparatus that is described in detail elsewhere (Verkman et al., 1980). A 4°C temperature increment was obtained within 4 μs by discharging a 0.1-μF capacitor charged to 15,000 V across a 0.8-ml solution volume. The instrument resolution time was ~5 μs. The initial sample temperature was controlled to within 0.1°C by circulating water through the stainless steel electrodes, which were drilled hollow to within 60 μm of the tip. The binding of DBDS to erythrocyte ghosts was followed by measuring the fluorescence at an excitation wavelength of 356 nm and emission wavelengths >410 nm as transmitted by two 3-144 optical filters (Corning Glass Works, Corning, NY). Data were recorded on a Biomation (Cupertino, CA) 805 waveform recorder and transferred to a PDP 11/34 computer for storage on disk and numerical analysis.

Stopped-Flow Studies

Stopped-flow experiments were performed on an apparatus consisting of two hand-driven syringes which propelled solutions into a dual-jet-stream mixing chamber and observation cell. The mixing chamber and observation cell were designed to replace the existing temperature-jump electrodes so that the same optics, fast electronics, and data acquisition equipment could be used. The stopped-flow instrument had a dead time of 60 ms as determined by the reaction of $Fe(NO_3)_2$ with KSCN. The amount of DBDS that was bound to ghosts was measured by observed DBDS fluorescence intensity as in the temperature-jump experiments. A lucite box surrounded the entire stopped-flow apparatus so that the ambient temperature could be controlled by circulating air. Combined stopped-flow, temperature-jump experiments were performed on an apparatus described elsewhere (Verkman et al., 1981).

Comparison of Results of Temperature-Jump and Stopped-Flow Experiments

As discussed in the final section of this paper, a systematic difference was found between results obtained by these two methods. Consequently, a number of control experiments were carried out to see if the differences between the two methods could be attributed to artifacts peculiar to one of the techniques.

We first made a systematic investigation of the temperature-jump system. It is possible that the 15-kV pulse discharged across the temperature-jump cell could damage the red cell ghosts, since Tessie and Tsong (1980) have shown that much smaller voltage jumps can punch holes in red cell membranes. Several types of experiments were performed. When a sample was subjected to as many as 10 temperature jumps, the relaxation time, observed after each temperature jump (see Eqs. 2 and 3 and accompanying discussion), did not change significantly (data not shown). This experiment showed both that the temperature-jump method was reproducible and that the temperature jump did not cause a long-term degradation in the membrane. When the temperature-jump increment was varied, the relaxation amplitude was proportional to $(\text{voltage})^2$, as expected for a simple temperature-induced (in contrast to voltage-induced) perturbation. To search for possible temperature-induced

perturbations in band 3 structure, a stopped-flow, temperature-jump experiment was performed. The application of a temperature jump immediately before the DBDS-band 3 conformational change had no effect on the subsequent stopped-flow rate for the conformational change (Verkman et al., 1981), which implies that there are no significant temperature-induced relaxations in band 3 that are important in the present DBDS experiments.

The top section of Fig. 1 shows that as many as 16 temperature jumps had little effect on the stopped-flow time constant. This set of experiments indicates that the perturbation of the voltage and the sudden jump in temperature were not responsible for the difference between the two methods.

The major systematic errors in the stopped-flow measurements were expected to arise from sample heterogeneity and the presence of unstirred layers. Sample heterogeneity was investigated by measuring ghost size distribution in a fluorescence-activated cell sorter (FACS II; B-D FACS Systems, Sunnyvale, CA). The size distribution of washed ghosts was measured and a single gaussian distribution was observed in both citrate and chloride buffer. Furthermore, stopped-flow experiments performed with right-side-out (ROV) red blood cell vesicles gave essentially the same kinetic data as ghosts (data not shown). A single gaussian distribution of ROVs was observed; their volume is $\sim 10^{-13}$ cm^3 (Sze and Solomon, 1979), much smaller than the 10^{-10} cm^3 volume of ghosts (Levin et al., 1980). These results indicate not only that the preparations are homogeneous, but also that the size of the particle does not affect the result.

It was possible to make a simulation[1] to determine how thick an unstirred layer would be required to account for the discrepancy between temperature-jump and stopped-flow results. The presence of a 75-μm unstirred layer would resolve the discrepancy, as shown by the ×'s in Fig. 1. This is an unreasonably large unstirred layer thickness, since red cell membranes have been shown to have an unstirred layer thickness of 5.5 μm (Sha'afi et al., 1967) in a stopped-flow apparatus similar to ours. Furthermore, as Fig. 1 (bottom) shows, a 75-μm unstirred layer would cause a lag in the time course that would have been easily detectable in our apparatus.[1] Experiments performed in buffer containing 30% sucrose, which has three times the viscosity of water, gave a reaction time course within 20% of that observed without sucrose. Since the effect of the unstirred layer would be proportional to viscosity, these experiments showed that unstirred layers were not rate limiting. The results of these several types of control experiments led us to conclude that the differences between temperature-jump and stopped-flow experiments were not caused by any artifacts in the technique that we were able to identify.

RESULTS AND DISCUSSION

Equilibrium Binding

Our previous studies of the equilibrium binding of DBDS to ghost membranes suspended in 28.5 mM sodium citrate, pH 7.4 (160 mM ionic strength), clearly showed high-affinity (equilibrium constant, K_1^s) and low-affinity (K_2^s) DBDS binding sites (Dix et al., 1979). This result is in contrast to previous findings in other laboratories that showed DBDS, DNDS, and a dihydro analogue of DIDS, H_2DIDS (4,4′-diisothiocyano-2,2′-disulfonic dihydrostilbene), to have

[1] Verkman, A. S., and J. A. Dix. Effect of unstirred layers on binding and reaction kinetics at a membrane surface. Manuscript submitted for publication.

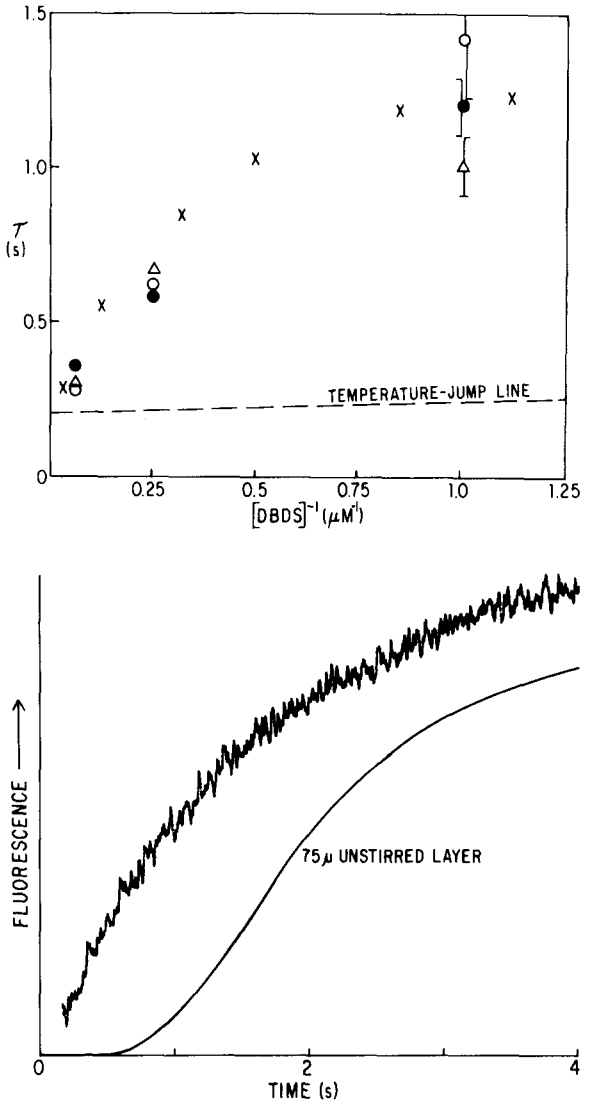

FIGURE 1. (Top) Effect of multiple temperature jumps and unstirred layers on DBDS-band 3 kinetics as measured by stopped-flow. A 0.8-ml sample of ghosts (1 mg/ml ghost protein) was temperature-jumped by passing 15,000 V across a 1.0-cm solution within 4 μs. The sample was temperature-jumped 0 (○), 8 (●), and 16 times (△). The ghost solution was then diluted to a concentration of 0.04 mg/ml ghost protein and mixed with DBDS in a stopped-flow experiment. The observed exponential time constant is plotted in the top figure. The dashed temperature-jump line indicates where data would fall on this plot if parameters obtained by temperature jump were correct. The points marked × show where the stopped-flow time constants would fall if the temperature-jump parameters were correct and if there were a 75-μm unstirred layer. (Bottom) Effect of 75-μm unstirred layer. The bottom figure contrasts typical experimental stopped-flow data (0.5 μM DBDS, 0.02 mg/ml ghost protein) with a simulated stopped-flow time course assuming a 75-μm unstirred layer and temperature-jump kinetic parameters. The experimental trace has been displaced from the origin by an amount equal to the dead time of the stopped-flow apparatus.

a single class of binding sites on the red cell membrane as determined by equilibrium binding and kinetic measurements (Fröhlich and Gunn, 1980; Rao et al., 1979; Barzilay and Cabantchik, 1979; Shami et al., 1978). There are considerable differences in the ionic strength and the ionic composition of the buffers used in these measurements, and it has now become apparent that each of these factors has an effect on DBDS binding. To examine these factors separately, we first studied the effect of ionic strength at a constant pH of 7.4 using citrate as the sole component of the buffer. We have also studied the effect of chloride in a second set of experiments, at constant ionic strength and pH, and these results will be reported in a subsequent paper.

Fig. 2 gives a Scatchard plot of the results at 28.5 mM citrate, obtained by centrifugation, to be compared with those obtained by fluorescence enhancement titration (insert). The stoichiometry can be determined from the centrifugation measurements, which yield the value of 3.2 ± 0.3 nmol/mg; this stoichiometry was used to normalize the fluorescence enhancement points in the insert. It agrees with the value of 2.7 nmol/mg given previously (Dix et al., 1979) and that of 2.5 nmol/mg for BIDS (4-benzamido-4′-isothiocyano-2,2′-disulfonic stilbene) given by Rao et al. (1979). Our stoichiometry is equivalent to 1.2×10^6 sites/cell (computed on the basis of 6.0×10^{-10} mg protein/ghost; Dodge et al., 1963), which agrees with the value of $1\text{–}1.2 \times 10^6$ sites/cell commonly accepted as the number of band 3 monomers (Knauf, 1979; Passow et al., 1980).

There is a discrepancy[2] between the present results and those previously given by Dix et al. (1979); no points from the Dix paper have been included in Fig. 2. We believe the present data to be representative of the preparations in the present paper, in part because of the very large number of data points taken in the centrifugation experiments (72 points) and in part because of the agreement with the fluorescence data (six experiments). A nonlinear fit to the 72 centrifugation points in Fig. 2 gives two apparent dissociation constants: $K_1^s = 110 \pm 51$ nM as the high-affinity constant and $K_2^s = 980 \pm 200$ nM as the low-affinity constant. The value of K_1^s given by the fluorescence method is 65 ± 8 nM (range 50–80 nM, six experiments) and that of $K_2^s = 820 \pm 100$ nM for the low-affinity site. Since the fluorescence method has much less scatter than centrifugation, the apparent dissociation constants from the fluorescence method have been used in all the subsequent calculations in this paper.

We have also used the fluorescence enhancement data to apply the variance

[2] The data from the previous experiments of Dix et al. (1979) are different from the present data, possibly because of a systematic difference in procedure that we have not been able to identify. In those experiments, 17 data points were obtained and the data give $K_1^s = 28 \pm 4$ nM, which is the appropriate value for comparison with the value of $K_1^s = 65 \pm 8$ nM given in the present paper. 28 nM is one-half of the 56 nM value published by Dix et al. and is the correct value of K_1^s, when discussing apparent binding affinities, which are used in the present paper, rather than intrinsic binding affinities, which were used in the Dix paper to describe the sequential mechanism. A similar correction is required to determine K_2^s which is 3.7 μM when expressed as an apparent binding affinity. This value is very much greater than the present value of 0.82 ± 0.1 μM. As Fig. 1 of Dix et al. (1979) shows, the low-affinity binding constant was not well resolved.

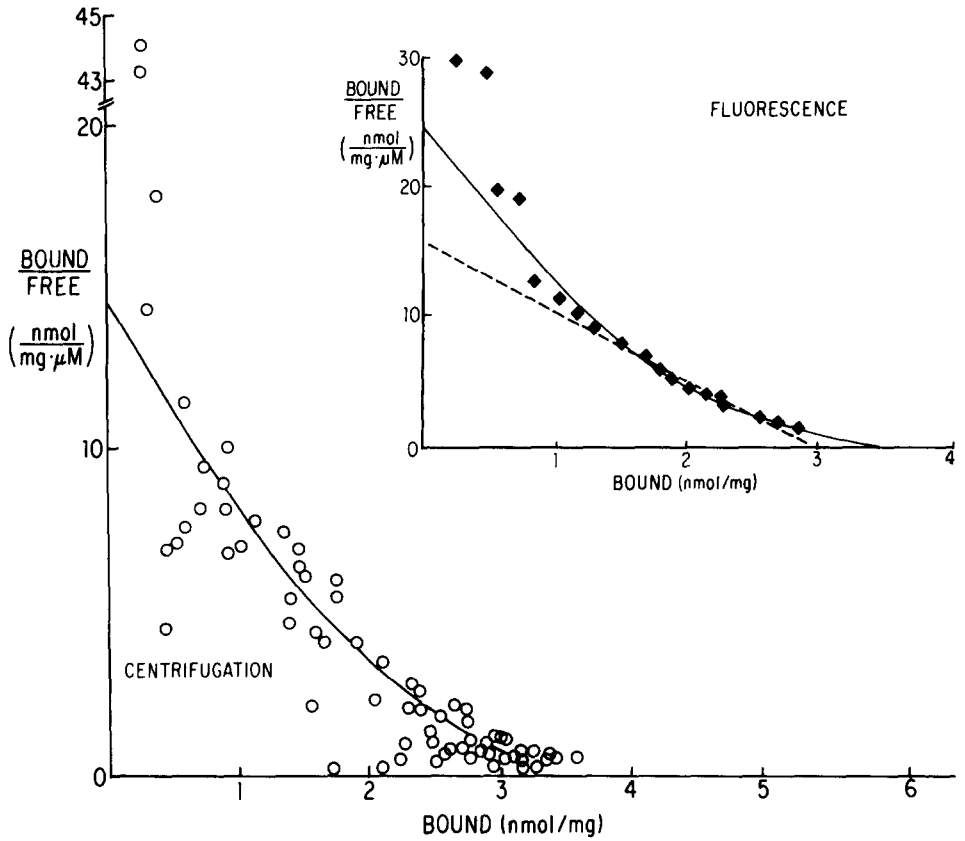

FIGURE 2. Scatchard plots of equilibrium binding of DBDS to ghosts. Equilibrium binding data taken by the centrifugation method are shown at the left. Each of the 72 data points is an average of experiments performed in duplicate or triplicate. The abscissa is calculated from the difference between total ghosts added and the quantity of bound DBDS determined as described in Materials and Methods. The ordinate is the ratio of calculated bound DBDS to measured free supernatant DBDS. The curve drawn through the data represents a three-parameter fit to a two-site, sequential-binding model,

$$\frac{B}{F} = \frac{(K_2^s/2 + F)v}{K_1^s K_2^s + K_2^s F + F^2},$$

where v is the total site stoichiometry, 3.2 nmol/mg protein, as given in the text, B is bound DBDS, F is free DBDS, and K_1^s and K_2^s are the high- and low-affinity binding constants, as detailed in Eqs. A1–A4 and A9 in the Appendix. In the fitting procedure, B is expressed as a function of F and all F points are assigned equal statistical weight. Fluorescence binding data are shown in the insert. The method to calculate the Scatchard representation from fluorescence data is given in the Appendix (Eqs. A1–A4, A9, and A10) and involves using the value of v from the centrifugation data and the same weighting procedure. The fitted curve is determined in the same manner as for centrifugation data. The dashed line in the fluorescence plot was obtained from a single binding site fit to the data; the B/F vs. F data were fitted to a straight line with individual points weighted inversely to the B/F value.

ratio test (F test) to determine whether a two-site, sequential model, in which there are three adjustable parameters, fits the data better than a single-site model with two adjustable parameters. The dashed straight line in the inset in Fig. 2 shows the least-squares fit for a single site, weighting individual points inversely to the bound/free value. The F test was carried out by comparing χ^2 for this line with that for a fit to the sequential model, using the same weighting procedure and making the normal compensation for the difference in degrees of freedom. The P value for the model, which includes the third parameter, is 0.006 (F = 3.56), which means that the sequential-binding model fits the data significantly better than a single-site model. Furthermore, if the data points are weighted equally, the sequential binding model still fits the data better than a single-site model ($P = 0.03$; F = 2.52). Thus, the F test justifies the choice of a two-site model over the single-site model. The F test does not address the question of whether the two sites should be described by a sequential-site or an independent-site model, which is discussed below in the section on the analysis of temperature-jump data.

The results at five ionic strengths are shown in the double-reciprocal plot of Fig. 3. The characteristic curvature near the origin, observed when more than one site is involved,[3] is only barely apparent at the lowest citrate concentrations in a double-reciprocal plot (cf. Rao et al., 1979), in contrast to the Scatchard plot in Fig. 2 in which the contribution of both sites is clearly evident. A nonlinear least-squares fit to the data, as described in the Appendix, characterizes the two binding sites at 5 mM citrate, which are described by $K_1^s = 0.48 \pm 0.05$ μM and $K_2^s = 8 \pm 1$ μM.

Fig. 4 shows that both dissociation constants, K_1^s and K_2^s, decrease as ionic strength increases. Since DBDS binding to both sites increases with increased citrate concentration, there can be no simple competition between citrate and DBDS for these sites. If the ionic strength effect were due to electrostatic interactions characteristic of homogeneous solutions, the association constant would be expected to depend logarithmically upon the square root of ionic strength. Since Fig. 4 shows this relation to be satisfied by both sites, the attraction between the stilbene inhibitor and the band 3 sites can be understood in terms of the decrease in the Debye length as ionic strength increases, although other explanations are not excluded. It is also significant that, although the apparent affinities of the two sites differ by a factor of ~10, their dependence upon ionic strength is the same, since the slopes of the lines, given in the legend to Fig. 4, do not differ significantly. Thus, though the fine structure of the binding process depends upon the specific molecular configuration of each site, the approach to the sites depends upon electrostatic interactions in the vicinity that are common to both.

Citrate was used in these studies to provide a model system in which the observations were not complicated by anion transport (see Rothstein et al., 1976). The underlying assumption is that the three negative charges of citrate prevent its transport by the anion exchange system. At pH 7.40, as used in all of our measurements, 1.1% of the citrate molecules are doubly charged and

[3] In the presence of chloride, there is only one apparent DBDS site (Verkman, 1981) in agreement with the observations of Fröhlich and Gunn (1980) with DNDS.

only 0.003% are singly charged. Since doubly charged molecules like sulfate are transported much more slowly than singly charged anions, transport of the doubly charged citrate ions should be negligible.

It is also possible for citrate to interact with the binding sites, though the effect is not large. Schnell et al. (1978) have concluded that citrate exercises little effect on the concentration dependence of chloride self-exchange. These authors also cite experiments in which citrate added to the outside of the red cell inhibited unidirectional chloride flux with an inhibition constant of 125

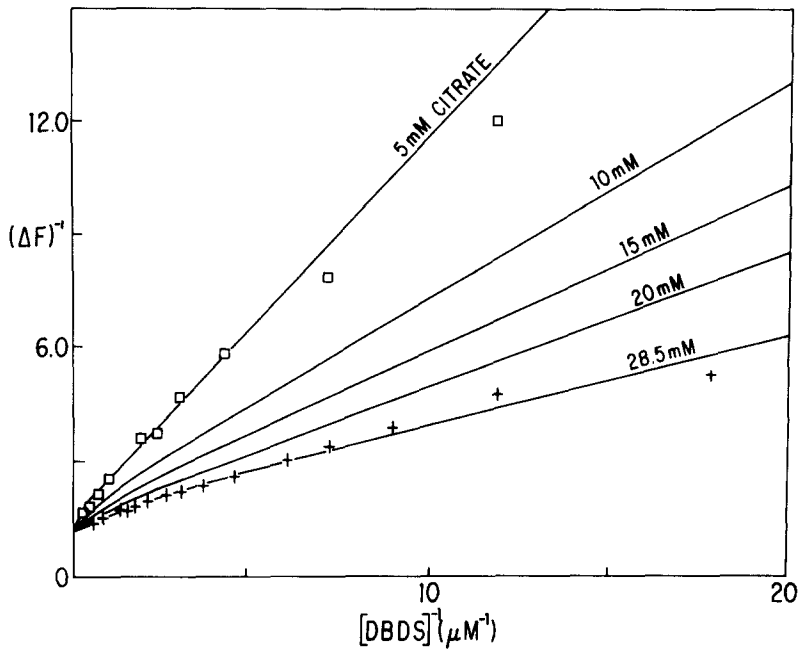

FIGURE 3. Double-reciprocal plot of equilibrium binding of DBDS to ghost membranes. The ordinate is the inverse of the corrected fluorescence (ΔF) of DBDS bound to ghost membranes in 5–28.5 mM citrate, pH 7.40, determined as described in the Appendix. The abscissa is the inverse of the total DBDS concentration in the ghost suspension so that the relative errors are smallest near the origin. The lines have been drawn by a nonlinear least-squares fit to the data using the sequential-binding model. For clarity, the data points for the intermediate citrate concentrations have been omitted.

mM, much higher than our maximum concentration of 28.5 mM. However, these experiments were not all carried out at constant ionic strength, so that the conclusions may depend upon factors other than citrate concentration. Nonetheless, the absence of any effect at citrate concentrations in the range that we have used suggests that citrate binding to the transport site is not an important factor.

These findings do not rule out an interaction between citrate and the DBDS site because the transport site may not be the DBDS binding site (Passow et

al., 1980; see also Verkman et al., 1982). Consequently, we carried out studies with sodium gluconate, which Fröhlich and Gunn (1980) had used as a passive anion to maintain ionic strength. The data shown in Fig. 5 for one experiment, typical of three, indicate that DBDS binding in the presence of gluconate is characterized by two binding sites with $K^s_{1,\text{gluc}} = 52 \pm 10$ nM and $K^s_{2,\text{gluc}} =$

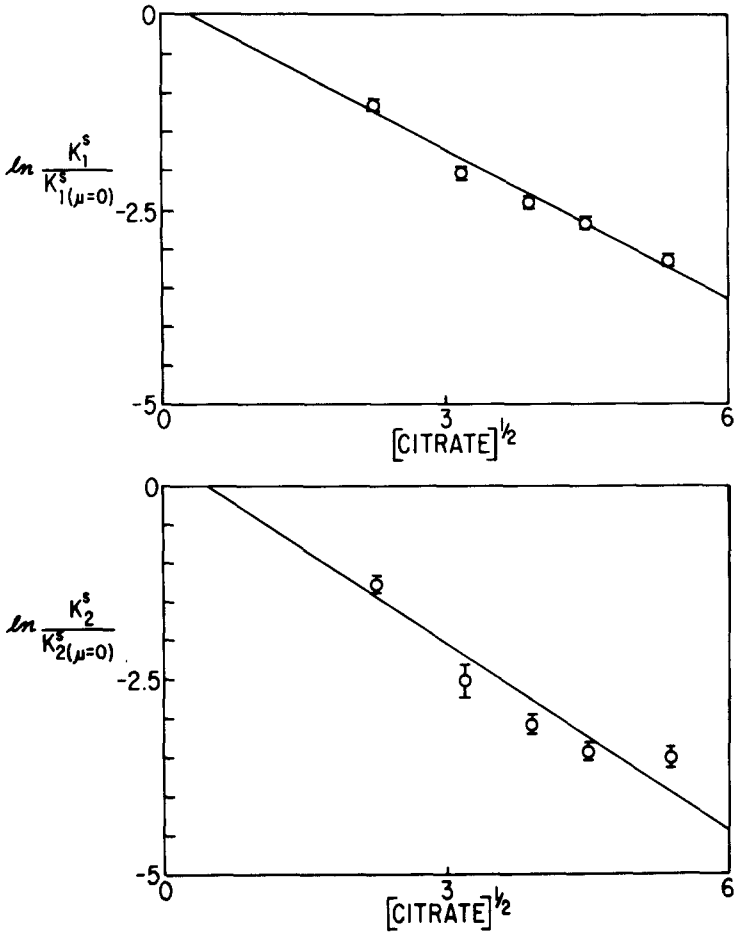

FIGURE 4. Effect of ionic strength, μ, on the dissociation constants, K^s_1 and K^s_2. The lines were drawn by weighted linear least-squares. The line in the upper graph for K^s_1 has a slope = -0.64 ± 0.06 $mM^{-1/2}$, $r = 0.99$; that for K^s_2 in the lower graph has a slope of -0.81 ± 0.14 $mM^{-1/2}$, $r = 0.96$. Error bars represent 1 SD from the mean and range from 5 to 18%.

400 ± 100 nM. The apparent dissociation constant for the high-affinity site is essentially the same with gluconate as citrate ($K^s_1 = 65 \pm 8$ nM), whereas that for the low-affinity site may differ ($K^s_2 = 820 \pm 100$ nM). It is technically difficult to measure affinities in the presence of gluconate because it produces a great deal of scattering and so we have not been able to determine $K^s_{2,\text{gluc}}$

accurately. To the accuracy of our measurements, binding of DBDS in the presence of gluconate is qualitatively similar to that in citrate. Small differences between gluconate and citrate binding would not be surprising since for the same ionic strength there are five times as many gluconate as citrate molecules. Both the charge distribution and the steric restrictions appropriate to the dimensions of the binding site within the membrane could well affect binding in the presence of two such disparate solutes.

The purpose of establishing a model system based on citrate is to provide

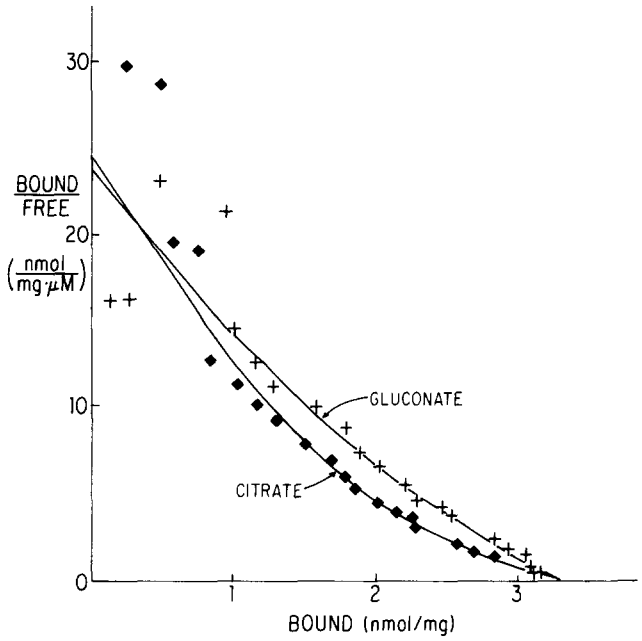

FIGURE 5. Scatchard plot of the effect of gluconate on equilibrium binding of DBDS. The binding of DBDS to band 3 in ghost membranes was measured at 155 mM gluconate (plus 25 mM glycylglycine, pH 7.40) (+) and 28.5 mM citrate, pH 7.40 (◆), by the fluorescence titration method. The citrate data and fitted curve are identical to those shown in Fig. 2; the curve through the gluconate data was obtained by a fit to the sequential-binding model in a manner identical to the fit for citrate data.

a benchmark against which the perturbations introduced when Cl is added to the system can be measured. The observations of Schnell et al. (1978) indicate that binding of citrate to the transport site is relatively unimportant. Our finding that DBDS binding in the presence of gluconate is not grossly different from that with citrate supports the view that specific citrate interactions with band 3 do not introduce significant distortion into our conclusions. Hence, it seems justifiable to consider citrate as an essentially inert component in our model system.

Several experiments suggest that the high- and low-affinity DBDS binding

sites are located on band 3. Experiments were carried out with ghosts prepared from red cells in which >95% of anion transport was inhibited by covalent reaction with DIDS (Knauf, 1979). Fig. 6 shows that ghosts covalently labeled with DIDS have no detectable DBDS binding sites as measured by fluorescence enhancement. The temperature-jump response also disappears, as shown in Fig. 7. No fluorescence signal was observed in temperature-jump experiments in which DBDS was mixed with vesicles prepared from lipids extracted from red blood cells, as shown in the bottom trace. As previously pointed out, the maximum labeling by the covalent DBDS analogue BIDS is 2.5 nmol/mg ghost protein, which is approximately twice as large as the stoichiometry for

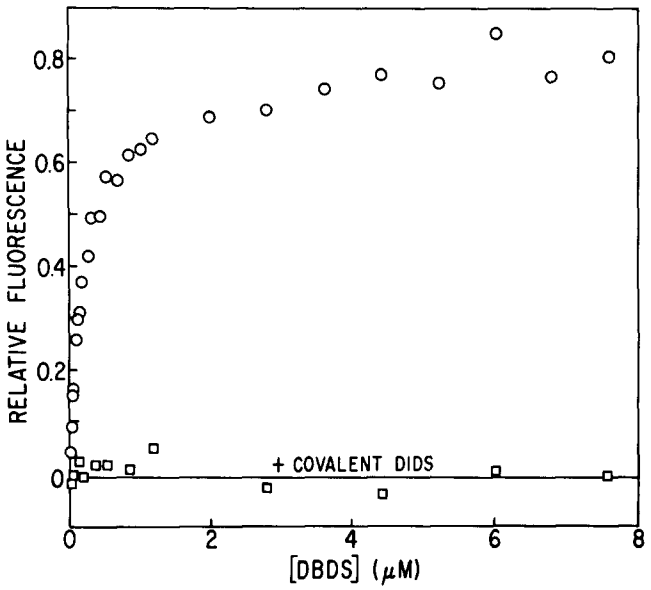

FIGURE 6. Effect of covalent DIDS on DBDS binding to ghosts. Fluorescence binding data were obtained from DBDS binding to band 3 in ghosts (○) and for DBDS binding to ghosts made from cells labeled covalently with DIDS (□), in which anion exchange was >95% inhibited as measured by SO_4 exchange at pH 6.3. The line is drawn for zero relative fluorescence.

the low-affinity site of 1.6 nmol/mg protein and entirely consistent with the accommodation of both sites on band 3. Taken together, these results strongly support the view that all of the high-affinity sites and low-affinity sites are located on band 3.

Stopped-Flow Studies

An advantage of a stopped-flow experiment over a temperature-jump experiment is that forward and reverse rates can be uncoupled. We used this feature in designing a set of experiments to see if the limiting behavior of the system conformed to the general predictions of Eq. 1. A qualitative test of the

mechanism is the dependence of the stopped-flow time constants on band 3 and DBDS concentrations. The observed time constant of such a system is given by (Czerlinski, 1966):

$$\tau^{-1} = k_{-2} + \frac{k_2 [\text{DBDS}]_{\text{tot}}}{K_1 + [\text{DBDS}]_{\text{tot}}}, \quad (2)$$

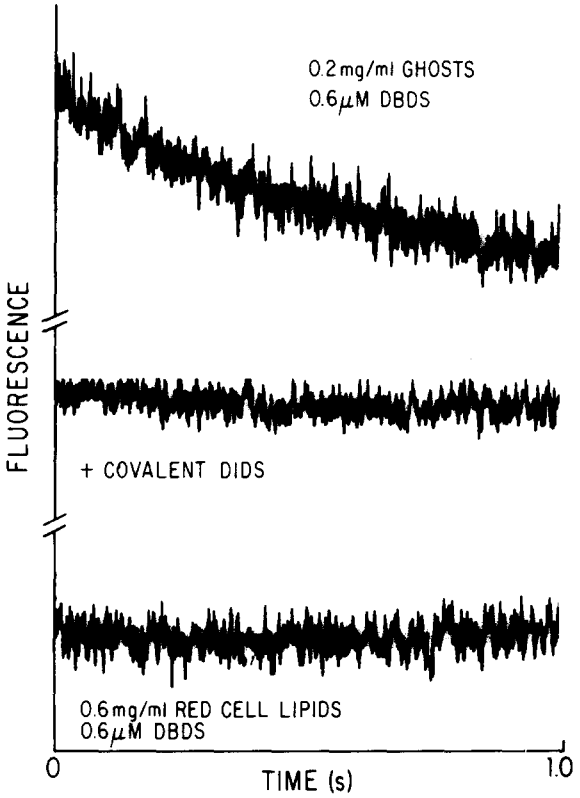

FIGURE 7. Effect of covalent DIDS on the time course of DBDS binding to ghosts. The upper trace shows a temperature jump of 0.2 mg/ml ghosts + 0.6 μM DBDS in 28.5 mM sodium citrate, pH 7.4, initial temperature 23°C. Decreased fluorescence corresponds to unbinding of DBDS from ghosts induced by the temperature jump. The upper trace was fitted to a single exponential to give a time constant of 0.25 ± 0.03 s. The middle trace shows that a temperature jump of 0.6 μM DBDS in 0.2 mg/ml ghosts treated covalently with DIDS as described in the legend to Fig. 6 gave no fluorescence enhancement. A similar result was found when 0.6 mg/ml lipids were treated with 0.6 μM DBDS as shown in the bottom trace.

when the total DBDS concentration, $[\text{DBDS}]_{\text{tot}}$, is very much larger than the total band 3 concentration, $[\text{band 3}]_{\text{tot}}$. This condition is fulfilled for the data in groups A–C in Table I. Eq. 2 is derived on the basis of a symmetrical bimolecular association so that when $[\text{band 3}]_{\text{tot}}$ is very much larger than $[\text{DBDS}]_{\text{tot}}$, as in group D, an equation analogous to Eq. 2 can be used in

which $[\text{band 3}]_{tot}$ replaces $[\text{DBDS}]_{tot}$. When the concentrations are comparable, as in group E, a full numerical solution is required. The values of τ^{-1} were determined by a nonlinear least-squares fit of a single exponential to the stopped-flow time course; the fit to Eq. 2 is good for groups A–D, in which the reduced χ^2 values ranged between 1.0 and 1.3.

When $[\text{DBDS}]_{tot}$ is large, as in group A, τ^{-1} becomes independent of $[\text{DBDS}]_{tot}$ and approaches the limiting temperature-jump relaxation rate, 5.5 s^{-1}. For small values of $[\text{DBDS}]_{tot}$ (although larger than $[\text{band 3}]_{tot}$), as in group B, τ^{-1} is linearly related to $[\text{DBDS}]_{tot}$. In group C there is little dependence of τ^{-1} upon $[\text{band 3}]_{tot}$ because $[\text{DBDS}]_{tot}$ is constant and Eq. 2

TABLE I

RESULTS OF STOPPED-FLOW STUDIES*

Conditions	Group	$[\text{DBDS}]_{tot}$	$[\text{Band 3}]_{tot}$	τ^{-1}
		μM	μM	s^{-1}
Large $[\text{DBDS}]_{tot}$	A	40	0.25	3.70±0.41
		20	0.25	4.00±0.32
		10	0.25	2.78±0.23
Small $[\text{DBDS}]_{tot}$	B	1.27	0.071	0.67±0.22
		0.86	0.071	0.46±0.06
		0.43	0.071	0.29±0.04
Constant $[\text{DBDS}]_{tot}$	C	3.27	0.78	1.27±0.02
		3.27	0.078	1.25±0.05
		3.27	0.015	1.32±0.09
Large $[\text{Band 3}]_{tot}$	D	0.062	0.71	0.82±0.13
		0.072	0.78	0.74±0.03
		0.12	0.71	0.88±0.07
		0.12	0.36	0.60±0.11
$[\text{DBDS}]_{tot} \approx [\text{Band 3}]_{tot}$	E	0.36	0.78	0.71±0.04
		0.36	0.078	0.45±0.04
		0.43	0.36	0.75±0.11
		1.27	0.14	0.56±0.05

* $[\text{DBDS}]_{tot}$ and $[\text{band 3}]_{tot}$ refer to the total concentration of each component present after equal volumes of solution have been mixed. Each τ^{-1} is the average of four experiments; errors represent 1 SEM. $[\text{Band 3}]_{tot}$ was calculated from the stoichiometry of the sequential binding model.

applies because $[\text{band 3}]_{tot}$ is small compared with $[\text{DBDS}]_{tot}$. When $[\text{band 3}]_{tot} \gg [\text{DBDS}]_{tot}$, as in group D, τ^{-1} becomes independent of $[\text{DBDS}]_{tot}$, as expected from the modified Eq. 2, in which $[\text{band 3}]_{tot}$ replaces $[\text{DBDS}]_{tot}$. When the concentrations of the two components are comparable, as in group E, the conditions for the derivation of Eq. 2 are not fulfilled and the numerical solution described in the Appendix is required.

A useful way to analyze stopped-flow time constants is to transform Eq. 2:

$$\tau = \frac{K_1}{k_2}\frac{1}{[\text{DBDS}]_{tot}} + \frac{1}{k_2}. \tag{3}$$

This transformation is valid providing $k_2 \gg k_{-2}$ and $[\text{DBDS}]_{tot} \gg [\text{band 3}]_{tot}$

(see below). Thus, a linear fit of τ to $[DBDS]_{tot}^{-1}$ gives k_2 = 1/intercept, K_1 = slope/intercept and $k_{-2} = k_2/[(K_1/K_1^s) - 1]$. However, the accuracy can be improved by fitting the stopped-flow data in Table I using the nonlinear least-squares fitting procedure outlined in the Appendix, which gives $k_2 = 4.0 \pm 1.5$ s^{-1} and $k_{-2} = 0.09 \pm 0.02$ s^{-1}. Using the best-fit values of k_2 and k_{-2}, the values for the two equilibrium constants K_1 and K_3 of the sequential mechanism of Eq. 1 can be obtained since they are related to the two equilibrium binding constants K_1^s and K_2^s by

$$K_1^s = K_1/(1 + K_2); \tag{4}$$

$$K_2^s = K_3\,(1 + 1/K_2), \tag{5}$$

where $K_2 = k_2/k_{-2}$. The data obtained in this way are shown in Table II, which summarizes the kinetic and equilibrium parameters of the system.

TABLE II

KINETIC, EQUILIBRIUM, AND THERMODYNAMIC PARAMETERS* FOR DBDS BINDING TO BAND 3

	Value	Units	ΔG (25°C)	ΔH	ΔS
			kcal/mol	*kcal/mol*	*eu*
K_1	3.0±1.4	μM	−7.6±0.5	−6±2	5±1
k_2	4.0±1.5	s^{-1}	17§±6	5.3±1.6	−38±9
k_{-2}	0.09±0.02	s^{-1}	19§±6	12.2±2.4	−24±3
K_2	44±19	—	−2.2±0.3	−7±2	−16±4
K_3	0.85±0.1	μM	−8.3±1.1	−2.5±2.6	20±5
K_1^s	0.065±0.008	μM	−9.8±0.1	−13.1±3	−11±5
K_2^s	0.82±0.1	μM	−8.3±0.1	−2.5±2.6	20±5

* The values for k_2 and k_{-2} are those determined by the stopped-flow method and those for K_1 and K_3 are derived from these values and the equilibrium binding data by Eqs. 4 and 5.

§ The thermodynamic parameters refer to the activated state, that is, ΔG is $\Delta G‡$, ΔH is $\Delta H‡$, and ΔS is $\Delta S‡$.

Analysis of Temperature-Jump Data

When Dix et al. (1979) put forward the reaction scheme given in Eq. 1, they discussed the independent-site model given below as an alternative to the sequential-binding model:

$$\begin{array}{l} \text{band 3} \overset{K_1^i}{\rightleftharpoons} \text{band 3-DBDS} \underset{k_{-2}^i}{\overset{k_2^i}{\rightleftharpoons}} \text{band 3*-DBDS} \\ \qquad\qquad \downarrow \\ \qquad\quad \text{DBDS} \\ \\ \text{band 3} \overset{K_2^{i\,s}}{\rightleftharpoons} \text{band 3-DBDS} \\ \qquad\qquad \downarrow \\ \qquad\quad \text{DBDS} \end{array} \tag{6}$$

in which the superscript i denotes the independent-site model. At that time, they were unable to compare these two alternative models quantitatively.

However, a complete analysis of the data from 38 data points obtained by the temperature-jump method makes it possible to discriminate between them in terms of the goodness of fit of τ^{-1} over a broad concentration range of reactants, assuming the first bimolecular association to be fast compared with the conformational change. For each mechanism, an expression for the slow step can be derived by standard techniques (Czerlinski, 1966). In general,

$$\tau^{-1} = Ak_2 + Bk_{-2}, \tag{7}$$

where k_2 and k_{-2} are the forward and reverse rate constants for the slow step, and A and B (which are the coefficients of k_2 and k_{-2} in the Appendix, Eqs. A12 and A13) are mechanism-specific functions of [DBDS], [band 3], and equilibrium binding constants. For each mechanism, a weighted, nonlinear least-squares fit to the τ^{-1} data was performed. The equilibrium constants [DBDS] and [band 3] were fixed by the results of the equilibrium binding experiments and k_2 and k_{-2} were allowed to vary until the optimal fit was obtained. Fig. 8 shows a plot of $(\tau B)^{-1}$ as a function of A/B for the two mechanisms. The x and y positions for the 38 data points shown in each plot were calculated from the $[\text{DBDS}]_{\text{tot}}$ and $[\text{band 3}]_{\text{tot}}$, the measured τ^{-1} values, and the calculated values for A and B using parameters obtained from the nonlinear least-squares fit; the fitted values of k_2^{tj} (slope; the superscript tj denotes temperature-jump data) and k_{-2}^{tj} (intercept) give the lines drawn through the data. The points for the sequential-binding model (top figure) fit much better ($\chi^2 = 1.9$) than for the independent-site model (bottom figure, $\chi^2 = 6.2$). The best-fit values for k_2^{tj} ($5.5 \pm 0.2\ s^{-1}$) and k_{-2}^{tj} ($1.00 \pm 0.05\ s^{-1}$) agree with our previous values (Dix et al., 1979) of 4.4 and $1.0\ s^{-1}$.

The arguments that support the sequential-binding model[4] have all been based on the assumption that the first bimolecular association is fast compared with the conformational change. However, this assumption is only valid at high concentrations of DBDS compared with band 3, as will be shown in a subsequent section which makes a detailed comparison of the stopped-flow and temperature-jump results. When the DBDS concentration is comparable to the band 3 concentration, as in temperature-jump experiments, there is a discrepancy between results obtained with these two methods; this discrepancy disappears when the concentration of DBDS is much greater than that of band 3. To examine the effect of reactant concentration on the data in Fig. 8, filled circles have been used to denote those nine data points in which the velocity of the bimolecular association is fastest. As Fig. 8 shows, these filled circles fit the least-squares line for the sequential-binding model, which suggests that the arguments that favor the sequential-binding model are, to a first approximation, independent of the velocity of the bimolecular association.

[4] There are several other models that incorporate two binding sites and a conformational change. Mechanisms in which a slow conformational change precedes a fast bimolecular association of DBDS with band 3 are not consistent with the concentration dependence of the stopped-flow time constant (Table I). A conformation change following both DBDS associations is ruled out on the grounds that a signal is observed in stopped-flow experiments at low DBDS, when only the high-affinity site is occupied.

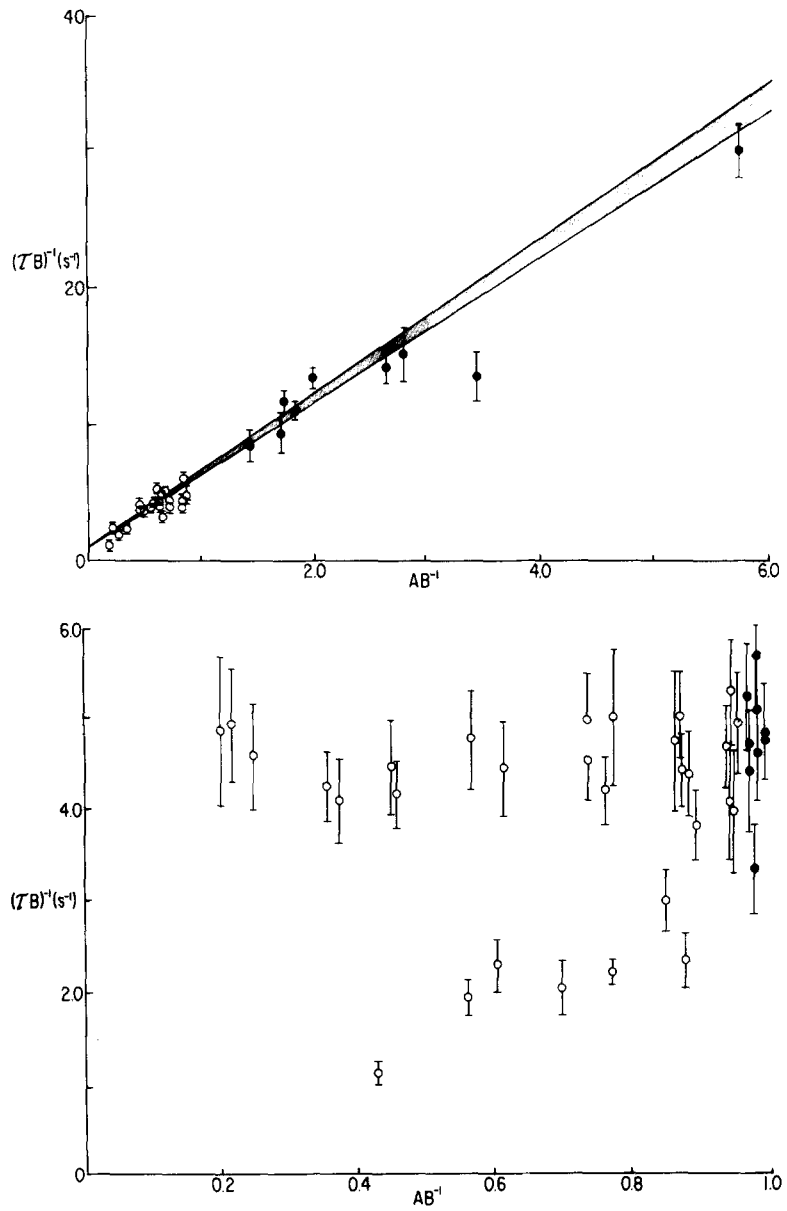

FIGURE 8. Concentration dependence of the temperature-jump relaxation times for sequential-binding and independent-site models. The top figure is computed for the sequential-binding model; the bottom one is for the independent-site model. The detailed expressions for A and B are given in the Appendix. The lines in the top figure were drawn with the kinetic constants obtained from a nonlinear least-squares fit of the relaxation expression, $\tau^{-1} = Ak_2 + Bk_{-2}$, to the temperature-jump data as described in the text and Appendix. Filled symbols represent data taken at the nine highest band 3 and DBDS concentrations, when [DBDS] >> [band 3]. The stippled segment in the sequential-binding model represents a zone within ±1 SD of the least-squares line.

Inside-out red blood cell vesicles (IOVs), as prepared by the method of Steck and Kant (1974), were used to study sidedness of DBDS binding to ghost membranes. When DBDS was added to an IOV preparation containing 70% IOVs and 30% right-side-out (ROV) vesicles, the equilibrium fluorescence intensity was 30 ± 4% of the intensity of a 100% ROV preparation having the same total protein concentration. If the 70% IOV preparation is incubated with DBDS at 23°C, the fluorescence slowly increases (over ~1 h at 1 μM DBDS) to the value obtained with 100% ROVs, corresponding to the slow permeation of DBDS through the IOV. These experiments suggest that the DBDS binding site involved in fluorescence enhancement is present only on the external red cell membrane surface.

Temperature Dependence

The enthalpies and entropies of the reactions in Eq. 1 that are given in Table II have been determined from the temperature dependence of the equilibrium constants (Fig. 9, top) and the stopped-flow rate constants (Fig. 9, bottom) for the conformational change. Jennings and Passow (1979) and Ramjeesingh et al. (1980) have shown that there is a single stilbene site per monomer. On the basis of this conclusion and the sequential reaction scheme, the thermodynamic parameters may be used to form a conceptual model of the mechanism by which the stilbene inhibitors interact with band 3.

The thermodynamic data are summarized in Fig. 10. Binding of the first DBDS molecule is a two-step process driven by two enthalpy changes of approximately equal magnitude. In our model the transition between the first step and the second step is effected by a conformational change in band 3 that internalizes the DBDS molecule within a cavity in band 3. We have found the transition to be very slow ($k_2 = 4\ s^{-1}$), which is consistent with a significant conformational change. It is accompanied by a large negative entropy of activation, equivalent to −11 eu, which we have attributed to the entropy change required to provide a hole large enough for the DBDS to penetrate to get closer to the charge on the site. Once the DBDS molecule has been internalized, band 3 relaxes to a less ordered state. The overall net enthalpy change for the first two steps is −13.1 kcal/mol, which provides the driving force for locking the first DBDS molecule into its position and more than compensates for the net entropy decrease equivalent to 3.4 kcal/mol. It is interesting that the final array after binding and internalization of the first DBDS is more ordered than when DBDS and ghost membranes are free in solution.

After the change in conformation has taken place, a second DBDS molecule can bind to its site on the second monomer. The major energetic component in this process is an increase in entropy, in contrast to binding of the first DBDS molecule, which is almost entirely enthalpy driven. Binding of the second DBDS molecule results in a decrease in the order of the system, as if the second DBDS did not fit in quite as neatly as the first. The difference in the driving forces between the two DBDS binding steps is consistent with the sequential-binding mechanism and not with two identical binding steps on two independent identical monomers. If the two sites were entirely in-

dependent and there was no interaction between the two monomers, the thermodynamic parameters for the K_1 and the K_3 process would be identical. Since they differ in driving force, there must be an interaction between the two monomers in order to modify the second site to have the characteristics revealed by the thermodynamic parameters.

These considerations lead us to view the band 3 dimer as an assembly of

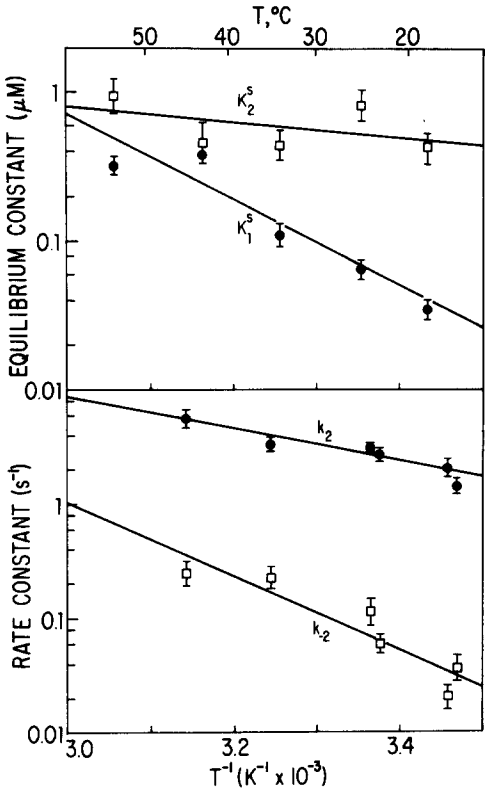

FIGURE 9. Temperature dependence of DBDS binding to band 3 in ghost membranes. All experiments were performed in 28.5 mM sodium citrate, pH 7.4. The two equilibrium binding constants, K_1^s and K_2^s, were obtained from fits to fluorescence enhancement data using the sequential-binding mechanism of Eq. 1 (one titration at each temperature). The rate constants, k_2 and k_{-2}, were obtained from stopped-flow experiments done (in quadruplicate) at various temperatures. Error bars represent 1 SE and the fitted line is a weighted linear least-squares fit to the data.

two identical monomers, each initially containing one site. The first DBDS chooses its site on either monomer. Once the conformational change in the first monomer is complete, the second monomer has also been transformed to provide a second site with the characteristics enumerated above. Nonetheless, the two sites have many characteristics that are basically similar, as shown by the similarity of the ionic strength dependence. This is consistent with a

common approach pathway to the site area, the final discrimination between the sites being provided by local changes in configuration. Our conclusions about cooperative interactions between the monomers support those put forward by Dix et al. (1979), Macara and Cantley (1981), and Salhany et al. (1981).

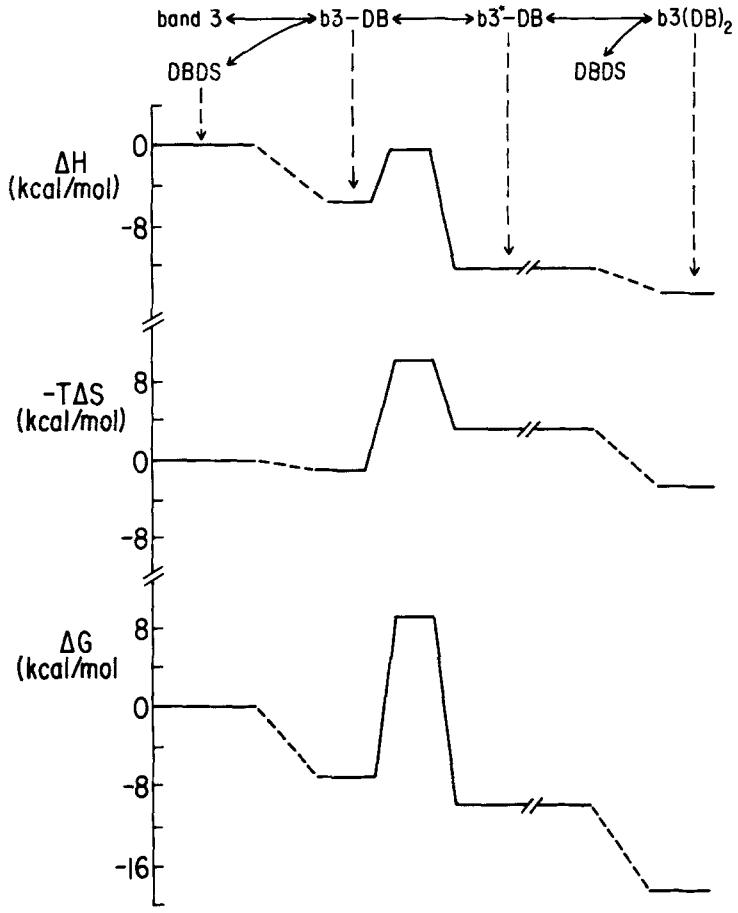

FIGURE 10. Thermodynamic energy profiles for DBDS binding to band 3 in ghost membranes. The energy profiles for the enthalpies and entropies of each stage of DBDS binding to band 3 (b3) are constructed from the temperature dependence of K_1^s, K_2^s, k_2, and k_{-2} shown in Fig. 9 and Table II. The equilibrium enthalpies and entropies were calculated from the slope and intercept of the logarithmic plot of the dissociation constants; the activation enthalpies and entropies were calculated as described by Glasstone et al. (1941).

Comparison of Stopped-Flow and Temperature-Jump Kinetics

A detailed comparison of the parameters computed on the basis of the reaction scheme in Eq. 1 shows that the kinetics given by the temperature-jump method are different from those given by stopped-flow. This is illustrated in

Fig. 11 in which the data from a stopped-flow experiment are plotted according to Eq. 3. The parameters obtained from the slope and intercept of the linear fit agree quite well with those given by the more accurate nonlinear least-squares fit. However, if these parameters were to be replaced by those given by the temperature-jump experiments, the agreement would disappear, as shown in the dashed line at the bottom of the figure. There is a large discrepancy that increases as the DBDS concentration is decreased. This means either that Eq. 1 (with two fast bimolecular steps) does not adequately

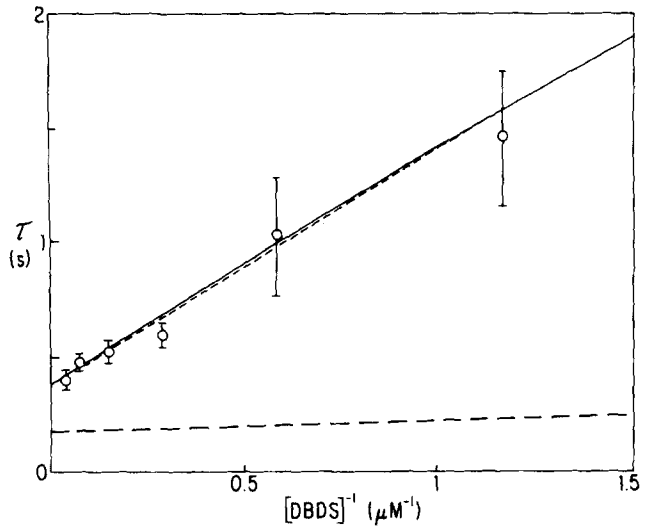

FIGURE 11. Comparison of stopped-flow and temperature-jump experiments. The points (○) are stopped-flow time constants obtained in a typical experiment (ghost protein concentration 0.03 mg/ml); the error bars represent the standard error of the mean. The solid line shows the best fit to the sequential-binding mechanism in which both bimolecular associations are fast. The lower dashed line represents the stopped-flow time constants expected, using the parameters obtained by the temperature-jump method, assuming two fast bimolecular associations. The upper dashed line shows the stopped-flow time constants that would be expected if the first bimolecular rate constant is slow, $5 \times 10^6\ M^{-1}\ s^{-1}$, as discussed in the text. Since the two upper lines do not differ significantly, the presence of a slow bimolecular step would not significantly alter the stopped-flow fit.

describe the kinetics of the system or that there is a systematic error in one or both of the methods.

Any systematic errors that caused a discrepancy between the two methods would be expected to arise from an artifact peculiar to one or the other of the methods. One such error could come from the unstirred layer, which is peculiar to the stopped-flow method, and another could be caused by perturbations introduced by the 15-kV discharge across the system that is peculiar to the temperature-jump method. These and other possible systematic errors

were examined in detail as described in Materials and Methods. Since we have been unable to find a systematic error, we have concluded that the probable basis for the difference is in the kinetic model given in Eq. 1.

In the earlier sections of the paper, the kinetics of the mechanism given in Eq. 1 were derived on the assumption that the bimolecular association step is fast compared with the conformational change. If this is not the case, and the velocity of the bimolecular association is comparable to that of the conformational change, there will be a much larger effect on temperature-jump than on stopped-flow measurements. The normal concentrations of DBDS used in the stopped-flow method are so high compared with band 3 concentrations that they drive the bimolecular association very fast compared with the velocity of the conformational change. In the temperature-jump experiments, useful data can be obtained only when the concentrations of band 3 and DBDS are comparable. Hence, in temperature-jump experiments, there is a significant contribution of the bimolecular association step to the observed relaxation time, so that the temperature-jump relaxation time constant reflects a combination of the bimolecular association and the conformational change.

A simulation procedure was used to determine the values of the rate constant, k_1, required to bring the temperature-jump data into agreement with stopped-flow. k_1 was obtained by fitting the temperature-jump data to the mechanism in Eq. 1, under conditions in which the bimolecular association is slow, keeping K_1, k_2, k_{-2}, and K_3 fixed to the values determined in stopped-flow experiments as given in Table II. Although the value of k_1 is not determined uniquely by this method (Dix and Verkman, 1982), typical values fall in the range $1\text{–}5 \times 10^6$ M^{-1} s^{-1}. The fit of the temperature-jump parameters to the stopped-flow data with $k_1 = 5 \times 10^6$ M^{-1} s^{-1} given by the upper dashed line in Fig. 11 shows that the inclusion of a slow first step does not significantly affect the analysis of the stopped-flow data. Although many other kinetic mechanisms have been examined unsuccessfully,[5] the fit of the

[5] Many modifications of the reaction scheme in Eq. 1 were considered in an attempt to determine the simplest reaction scheme that would resolve the stopped-flow temperatue-jump discrepancy. A fourth unimolecular reaction step was added to the sequential binding mechanism in Eq. 1 in four locations: a relaxation in band 3 occurring before the first DBDS addition, an additional conformational change occurring before and after the band 3-DBDS → band 3*-DBDS conformational change, and a conformational change in band 3*-DBDS making it unavailable to bind a second DBDS molecule. Several of these mechanisms have an important physical basis. For example, the band 3 conformational change occurring before DBDS is bound could correspond to the *cis-trans* motion of band 3 which exposes the anion binding site to the external and cytoplasmic surfaces, or, alternatively, to the outward- and inward-facing forms of band 3. Stopped-flow and temperature-jump data were simulated for each mechanism using the methods described by Dix and Verkman (1982). K_1^s and K_2^s were fixed from equilibrium binding experiments; k_2 and k_{-2} and a rate and equilibrium constant for the additional step were allowed to vary. Surprisingly, the additional degree of freedom allowed by a fourth reaction step did not resolve the discrepancy. A fourth step that was fast compared with the conformational change did not alter the analysis; therefore, the present methods cannot determine whether an additional fast conformational change exists. When the rates of the fourth step were comparable to or slower than the conformational change, the discrepancy between stopped-flow and temperature-jump data actually increased. In the presence of

slow bimolecular association version of Eq. 1 is not necessarily unique. It does represent, however, the simplest kinetic system that we have been able to use to resolve the discrepancy.

The rate constant of $\sim 10^6$ M^{-1} s^{-1} for the bimolecular association is some two orders of magnitude slower than the value of 10^8 M^{-1} s^{-1} which is characteristic of such reactions in free solution. One possible reason for the slow association would be steric hindrance in the access of DBDS to its binding site on band 3. Passow et al. (1980) have suggested that DBDS binds to a site some distance from the external face of the membrane, which is consistent with the finding of Rao et al. (1979) that the stilbene binding site is 30–45 Å from the internal membrane face. It has been suggested (Solomon et al., 1982) that the DBDS sites are located in an aqueous pore of ~4.5 Å radius situated between the two monomers of band 3. The tight fit of the bulky DBDS molecule into such an aqueous channel would be consistent with the slow bimolecular association that these calculations show.

APPENDIX

Equilibrium Binding Calculations

The equilibrium binding of DBDS to ghost membranes is described by four equations. For the sequential binding model, the equations are

$$K_1^s = \frac{[\text{DBDS}][\text{b3}]}{[\text{b3-DBDS}]}, \tag{A1}$$

$$K_2^s = \frac{[\text{b3-DBDS}][\text{DBDS}]}{[\text{b3-DBDS}_2]}, \tag{A2}$$

$$\text{b3}_T = [\text{b3}] + [\text{b3-DBDS}] + [\text{b3-DBDS}_2], \tag{A3}$$

$$\text{DBDS}_T = [\text{DBDS}] + [\text{b3-DBDS}] + 2[\text{b3-DBDS}_2], \tag{A4}$$

where [b3-DBDS] and [b3-DBDS$_2$] represent all conformations of band 3 with one and two DBDS molecules bound, respectively.

For the independent-site model, Eqs. A2–A4 are replaced with

$$K_2^{i,s} = \frac{[\text{b3}][\text{DBDS}]}{[\text{b3}'\text{-DBDS}]}, \tag{A5}$$

$$\text{b3}_T = [\text{b3}] + [\text{b3-DBDS}], \tag{A6}$$

$$\text{b3}'_T = [\text{b3}'] + [\text{b3}'\text{-DBDS}], \tag{A7}$$

$$\text{DBDS}_T = [\text{DBDS}] + [\text{b3-DBDS}] + [\text{b3}'\text{-DBDS}], \tag{A8}$$

---

chloride (20–150 mM), the discrepancy between stopped-flow and temperature-jump results disappears (J. A. Dix, A. S. Verkman, and A. K. Solomon, manuscript in preparation). In terms of the model presented above, this could correspond to an increase in the rate of the bimolecular association, or equivalently, a decrease in the activation energy barrier caused by the presence of chloride. This could occur if chloride binds to band 3 simultaneously with DBDS (see Verkman et al., 1982); bound chloride may alter the band 3 conformational state to reduce the binding activation energy.

where b3′ is the second independent site and $K_2^{i,s}$ is the dissociation constant for DBDS binding to b3′. $K_1^{i,s}$ is equal to K_1^s given in Eq. A1. The total band 3 concentrations are measured in units of milligrams per milliliter ghost protein; to convert to molar units, as needed to determine $b3_T$ and $b3'_T$, an additional equation is used:

$$b3_T^g = \gamma b3_T, \tag{A9}$$

where γ is a proportionally constant and $b3_T^g$ is the measured concentration of $b3_T$ in milligrams of protein per milliliter. For the centrifugation experiments, $b3_T^g$, $DBDS_T$, and [DBDS] are measured. The system of Eqs. A1–A4 (or A5–A8) and A9 can then be solved to obtain an expression containing three unknown parameters, K_1^s, K_2^s (or $K_1^{i,s}$, $K_2^{i,s}$), and γ. The centrifugation data were fitted using a nonlinear least-squares procedure to obtain K_1^s, K_2^s (or $K_1^{i,s}$, $K_2^{i,s}$), and γ.

In the fluorescence equilibrium binding experiments, the measured parameter is the fluorescence intensity, F, which contains contributions from bound DBDS ([bound]), free DBDS ([DBDS]), and scattering (S) multiplied by a correction factor, Q, which corrects for DBDS self-quenching and inner filter effects:

$$F = Q(\alpha\,[\text{bound}] + \beta[\text{DBDS}] + S) + C, \tag{A10}$$

where C is instrumental offset and α is the fluorescence intensity of bound DBDS; β and Q were determined by fitting the fluorescence intensity of free DBDS in the absence of ghosts to the quadratic $A[\text{DBDS}]^2 + \beta[\text{DBDS}] + D$. β is therefore the limiting fluorescence intensity per [DBDS] at low DBDS concentrations and Q is the correction ratio, $\beta/(\beta + A[\text{DBDS}])$. Q is between 0.99 and 1.00 for [DBDS] < 400 nM and is ~0.85 at 4 μM DBDS. S was determined from a direct measurement of the fluorescence intensity of a ghost solution in the absence of DBDS and was linearly corrected for ghost dilution as DBDS aliquots were added. S is multiplied by Q in Eq. A10 because scattered light intensity is reduced by DBDS absorption; all DBDS effects on self-quenching are assumed due to absorption of excitation or emission light. The total dilution for any given titration is <3%.

The six equations A1–A4 (or A5–A8), A9, or A10 that describe the fluorescence data can be solved; the measured values are $b3_T^g$, $DBDS_T$, β, Q, S, and C, and the four unknowns are K_1^s, K_2^s (or $K_1^{i,s}$, $K_2^{i,s}$), γ, and α. Attempts to fit the fluorescence data by a nonlinear least-squares procedure were not successful because the parameters γ and α were tightly coupled. We therefore fixed γ to the value obtained in the centrifugation technique and fit the data with three parameters to obtain K_1^s, K_2^s (or $K_1^{i,s}$, $K_2^{i,s}$), and α.

A second method can be used to fit the fluorescence data that does not rely on the value of γ. This method is applicable in the limit of low ghost concentration and was used to analyze the data in Fig. 3. Eq. A4 or A8 can be replaced with

$$[\text{DBDS}] = DBDS_T. \tag{A11}$$

The six equations describing the fluorescence data can then be solved to yield an expression containing three unknown parameters, K_1^s, K_2^s (or $K_1^{i,s}$, $K_2^{i,s}$), and α.

Temperature-Jump Calculations

The relaxation expressions for the sequential-binding and independent-site models are explained below. Each derivation assumes rapid equilibration for all binding steps (unless otherwise indicated) and a slow equilibration for the conformational step (Czerlinski, 1966). Each equation is written in the form $\tau^{-1} = Ak_2 + Bk_{-2}$ where A

and B are functions of the equilibrium constants, [DBDS], and high- and low-affinity binding site concentrations. For the independent site model, the high- and low-affinity sites are b3 and b3′, respectively; for the sequential model, the high- and low-affinity sites are b3 and b3*-DBDS. The rate constants for the slow conformational step, k_2 and k_{-2}, were determined from a least-squares fit of each equation to the temperature-jump data in Fig. 8. [DBDS], [b3], and [b3′] were calculated as described in the previous section. The dissociation constants in each model were held constant at the values determined in the equilibrium binding experiment. The lines through the data in Fig. 8 represent best fits to the data, allowing only k_2 and k_{-2} to vary for each model.

Sequential-Binding Model

$$\text{b3} \overset{K_1}{\longleftrightarrow} \text{b3-DBDS} \quad \underset{k_{-2}}{\overset{k_2}{\rightleftharpoons}} \quad \text{b3*-DBDS} \overset{K_3}{\longleftrightarrow} \text{b3*-(DBDS)}_2 \qquad \text{(A12)}$$

$$\text{DBDS} \qquad\qquad \text{DBDS}$$

$$\tau^{-1} = k_2\left(1 + \frac{[\text{DBDS}][\text{b3}] - K_1 a}{c}\right) + k_{-2}\left(1 + \frac{K_2[\text{b3}][\text{DBDS}] - b[\text{DBDS}]}{c}\right)$$

with $a = [\text{DBDS}] + K_3 + K_2[\text{b3}][\text{DBDS}]/K_1$; $b = [\text{b3}] + [\text{DBDS}] + K_1$;
$c = (ab - K_2[\text{b3}])^2[\text{DBDS}]/K_1$
and $K_2 = k_2/k_{-2}$; $K_1 = K_1^s(1 + K_2)$; $K_3 = K_2^s/(1 + 1/K_2)$.

Independent-Site Model

$$\text{b3} \overset{K_1^i}{\longleftrightarrow} \text{b3-DBDS} \quad \underset{k_{-2}^i}{\overset{k_2^i}{\rightleftharpoons}} \quad \text{b3*-DBDS} \qquad \text{b3}' \overset{K_2^{i,s}}{\longleftrightarrow} \text{b3}'\text{-DBDS} \qquad \text{(A13)}$$

$$\text{DBDS} \qquad\qquad\qquad\qquad \text{DBDS}$$

$$\tau^{-1} = k_2^i\left(\frac{[\text{DBDS}] + [\text{b3}]([\text{DBDS}] + K_1^i)/([\text{b3}'] + [\text{DBDS}] + K_2^{i,s})}{[\text{DBDS}] + [\text{b3}] + K_1^i}\right) + k_{-2}^i$$

with $K_2^i = k_2^i/k_{-2}^i$; $K_1^{i,s} = K_1^i(1 + K_2^i)$. $K_1^{i,s}$ and $K_2^{i,s}$ are the observed high-affinity and low-affinity dissociation constants when equilibrium binding data are fitted to an independent-site model.

Stopped-Flow Calculations

The differential equation for the sequential-binding mechanism was solved numerically (Dix and Verkman, 1982),

$$\frac{d[\text{b3*-DBDS}]}{dt} = k_2[\text{b3-DBDS}] - k_{-2}[\text{b3*-DBDS}], \qquad \text{(A14)}$$

with

$$\begin{aligned} K_1 &= [\text{b3}][\text{DBDS}]/[\text{b3-DBDS}] \\ K_3 &= [\text{b3*-DBDS}][\text{DBDS}]/[\text{b3*-(DBDS)}_2] \\ \text{b3}_T &= [\text{b3}] + [\text{b3-DBDS}] + [\text{b3*-DBDS}] + [\text{b3*-(DBDS)}_2] \\ \text{DBDS}_T &= [\text{DBDS}] + [\text{b3-DBDS}] + [\text{b3*-DBDS}] + 2[\text{b3*-(DBDS)}_2], \end{aligned} \qquad \text{(A15)}$$

subject to appropriate initial conditions. The observed fluorescence, $F(t)$, is the sum

of the fluorescent components weighted by enhancement factors, α_i,

$$F(t) = \alpha_1[\text{b3-DBDS}] + \alpha_2[\text{b3*-DBDS}] + \alpha_3[\text{b3*-(DBDS)}_2]. \quad \text{(A16)}$$

α_1 and α_2 were taken as unity and $\alpha_3 = 2$. The exponential time course of a stopped-flow experiment is independent of the α values, since all reactants in a coupled system with a single rate-limiting reaction have the same reaction time course.

To fit the i experimental time constants, $\tau_i \pm \Delta\tau_i$, to the best values for k_2 and k_{-2}, it was necessary to numerically generate a reaction time course for each value of k_2 and k_{-2}. The reaction time course was then fitted to a single exponential of time constant τ_i^f. The weighted sum of squared differences between τ_i and τ_i^f,

$$\chi^2 = \sum_i \frac{(\tau_i - \tau_i^f)^2}{(\Delta\tau_i)^2}, \quad \text{(A17)}$$

was minimized by varying k_2 and k_{-2} while keeping $K_1^s = K_1/(1 + k_2/k_{-2})$, $K_2^s = K_3(1 + k_{-2}/k_2)$ constant. Data fitted at temperatures other than 25°C were fitted by the same procedure while keeping K_1^s and K_2^s fixed at a value determined from the plot in Fig. 9.

We should like to express our thanks to Dr. Lewis Cantley not only for his collaboration in preparatory experiments from which the present study emerged, but also for continuing insightful discussion. Much of the apparatus was designed by Dr. Alfred Pandiscio and constructed by Mr. Bernard Corrow, to whom we are particularly indebted, as we are to Mr. Michael Toon for his technical assistance, particularly in the preparation of red cell ghosts and vesicles. This project was supported in part by National Institutes of Health grants 5R01 GM15692 and 2R01 HL 14820.

Received for publication 18 May 1981 and in revised form 19 October 1982.

REFERENCES

Barzilay, M., and Z. I. Cabantchik. 1979. Anion transport in red blood cells. II. Kinetics of reversible inhibition by nitroaromatic sulfonic acids. *Membr. Biochem.* 2:255–281.

Cabantchik, Z. I., P. A. Knauf, and A. Rothstein. 1978. The anion transport system of the red blood cell. The role of membrane protein evaluated by the use of "probes." *Biochim. Biophys. Acta.* 515:239–302.

Cabantchik, Z. I., and A. Rothstein. 1972. The nature of the membrane sites controlling anion permeability of human red blood cells as determined by studies with disulfonic stilbene derivatives. *J. Membr. Biol.* 10:311–330.

Czerlinski, G. H. 1966. Chemical Relaxation. Marcel Dekker, New York.

DeTar, D. F., and L. A. Carpino. 1956. The preparation and spectral characteristics of some 2-substituted *cis* and *trans* stilbenes. *J. Am. Chem. Soc.* 78:475–479.

Dix, J. A., and A. S. Verkman. 1982. Stopped-flow and temperature-jump measurements on biological systems: effects of heterogeneity, unstirred layers and multiple reaction intermediates. *Biophys. J.* 37:216*a*. (Abstr.)

Dix, J. A., A. S. Verkman, A. K. Solomon, and L. C. Cantley. 1979. Human erythrocyte anion exchange site characterised using a fluorescent probe. *Nature (Lond.).* 282:520–522.

Dodge, J. T., C. Mitchell, and D. J. Hanahan. 1963. The preparation and chemical characteristics of hemoglobin-free ghosts of human erythrocytes. *Arch. Biochem. Biophys.* 100:119–130.

Eigen, M., and L. DeMaeyer. 1974. Theoretical basis of relaxation spectrometry. *In* Investigation

of Rates and Mechanisms of Reactions. G. G. Hammes, editor. 3rd edition. Wiley-Interscience, New York. 63–146.

Fröhlich, O., and R. B. Gunn. 1980. Chloride transport kinetics of the human red blood cell studied with a reversible stilbene inhibitor. *Fed. Proc.* 39:1714.

Glasstone, S., K. J. Laidler, and H. Eyring. 1941. The Theory of Rate Processes. McGraw-Hill, New York. 524.

Huang, C., and T. E. Thompson. 1974. Preparation of homogeneous, single-walled phosphatidylcholine vesicles. *In* Methods in Enzymology. S. Fleischer and L. Packer, editors. Academic Press, Inc., New York. 32:485–489.

Jennings, M. L., and H. Passow. 1979. Anion transport across the erythrocyte membrane, in situ proteolysis of band 3 protein, and cross-linking of proteolytic fragments by 4,4′-diisothiocyanodihydrostilbene-2,2′-disulfonate. *Biochim. Biophys. Acta.* 554:498–519.

Kleinfeld, A. M., A. A. Pandiscio, and A. K. Solomon. 1979. A computer-controlled titration-fluorescence spectrometer. *Anal. Biochem.* 94:65–74.

Knauf, P. A. 1979. Erythrocyte anion exchange and the band 3 protein: transport kinetics and molecular structure. *Curr. Top. Membr. Transp.* 12:249–363.

Kotaki, A., M. Naoi, and K. Yagi. 1971. A diaminostilbene dye as a hydrophobic probe for proteins. *Biochim. Biophys. Acta.* 229:547–556.

Lepke, S., H. Fasold, M. Pring, and H. Passow. 1976. A study of the relationship between inhibition of anion exchange and binding to the red blood cell membrane of 4,4′-diisothiocyano stilbene-2,2′-disulfonic acid (DIDS) and its dihydro derivative (H_2DIDS). *J. Membr. Biol.* 29:147–177.

Levin, S. W., R. L. Levin, and A. K. Solomon. 1980. Improved stop-flow apparatus to measure permeability of human red cells and ghosts. *J. Biochem. Biophys. Methods.* 3:255–272.

Lowry, O. H., N. J. Rosenbrough, A. L. Farr, and R. J. Randall. 1951. Protein measurement with the Folin phenol reagent. *J. Biol. Chem.* 193:265–275.

Macara, I. G., and L. C. Cantley. 1981. Interaction between transport inhibitors at the anion binding sites of the band 3 dimer. *Biochemistry.* 20:5095–5105.

Passow, H., H. Fasold, E. M. Gärtner, B. Legrum, W. Ruffling, and L. Zaki. 1980. Anion transport across the red blood cell membrane and the conformation of the protein in band 3. *Ann. NY Acad. Sci.* 341:361–383.

Ramjeesingh, M., A. Gaarn, and A. Rothstein. 1980. The location of a disulfonic stilbene binding site in band 3, the anion transport protein of the red blood cell membrane. *Biochim. Biophys. Acta.* 599:127–139.

Rao, A., P. Martin, R. A. F. Reithmeier, and L. C. Cantley. 1979. Location of the disulfonic stilbene binding site of the human erythrocyte anion exchange system by fluorescence energy transfer. *Biochemistry.* 18:4505–4516.

Roelofsen, B., R. F. A. Zwaal, and C. B. Woodward. 1974. The action of pure phospholipases on native and ghost red cell membranes. *In* Methods in Enzymology. S. Fleischer and L. Packer, editors. Academic Press, Inc., New York. 32:131–140.

Rothstein, A., Z. I. Cabantchik, and P. Knauf. 1976. Mechanism of anion transport in red blood cells: role of membrane proteins. *Fed. Proc.* 35:3–10.

Salhany, J. M., E. D. Gaines, and R. Sullivan. 1981. Steady and transient state kinetics of erythrocyte anion exchange. Evidence for cooperativity in substrate and inhibitor binding suggesting site-site interactions within the band 3 protein dimer. *Biophys. J.* 33:3*a*. (Abstr.)

Schnell, K. F., E. Besl, and A. Manz. 1978. Asymmetry of the chloride transport system in human erythrocyte ghosts. *Pflügers Arch. Eur. J. Physiol.* 375:87–95.

Schulte-Frohlinde, D., H. Blume, and H. Gusten. 1962. Photochemical *cis-trans* isomerization of substituted stilbenes. *J. Phys. Chem.* 66:2486–2491.

Sha'afi, R. I., G. T. Rich, V. W. Sidel, W. Bossert, and A. K. Solomon. 1967. The effect of unstirred layers on human red cell water permeability. *J. Gen. Physiol.* 50:1377–1399.

Shami, Y., A. Rothstein, and P. A. Knauf. 1978. Identification of the Cl^- transport site of human red blood cells by a kinetic analysis of the inhibitory effects of a chemical probe. *Biochim. Biophys. Acta.* 508:357–363.

Ship, S., Y. Shami, W. Breuer, and A. Rothstein. 1977. Synthesis of tritiated 4,4′-diisothiocyano-2,2′-stilbene disulfonic acid ([^{3}H]DIDS) and its covalent reaction with sites related to anion transport in human red blood cells. *J. Membr. Biol.* 33:311–323.

Solomon, A. K., B. Chasan, J. A. Dix, M. F. Lukacovic, M. R. Toon, and A. S. Verkman. 1982. The aqueous pore in the red cell membrane: band 3 as a channel for anions, cations, nonelectrolytes and water. *Biophys. J.* 37:215*a*. (Abstr.)

Steck, T. L. 1978. The band 3 protein of the human red cell membrane: a review. *J. Supramol. Struct.* 8:311–324.

Steck, T. L., and J. A. Kant. 1974. Preparation of impermeable ghosts and inside-out vesicles from human erythrocyte membranes. *In* Methods in Enzymology. S. Fleischer and L. Packer, editors. Academic Press, Inc., New York. 31:172–180.

Sze, H., and A. K. Solomon. 1979. Permeability of human erythrocyte membrane vesicles to alkali cations. *Biochim. Biophys. Acta.* 550:393–406.

Tessie, J., and T. Y. Tsong. 1980. Evidence of voltage induced channel openings in Na/K ATPase of the human erythrocyte membrane. *J. Membr. Biol.* 55:133–140.

Verkman, A. S. 1981. The anion exchange system in the human red cell: a new method to study transport and inhibition mechanisms. M.D. Thesis, Harvard Medical School, Boston, MA.

Verkman, A. S., J. A. Dix, and A. A. Pandiscio. 1981. A simple stopped-flow temperature-jump apparatus. *Anal. Biochemistry.* 117:164–169.

Verkman, A. S., J. A. Dix, and A. K. Solomon. 1982. A non-competitive "shunt" pathway for the effect of chloride on the band 3-DBDS conformational change in red cell membranes. *Biophys. J.* 37:216*a*. (Abstr.)

Verkman, A. S., A. A. Pandiscio, M. Jennings, and A. K. Solomon. 1980. An improved temperature-jump apparatus. *Anal. Biochemistry.* 102:189–195.